The Interaction between Hurricane Opal (1995) and a Warm Core Ring in the Gulf of Mexico

XIAODONG HONG,*,@ SIMON W. CHANG,+ SETHU RAMAN,* LYNN K. SHAY,# AND RICHARD HODUR+

* *North Carolina State University, Raleigh, North Carolina*
+ *Naval Research Laboratory, Monterey, California*
# *Rosenstiel School of Marine and Atmospheric Science, University of Miami, Miami, Florida*

(Manuscript received 2 October 1998, in final form 27 April 1999)

ABSTRACT

Hurricane Opal (1995) experienced a rapid, unexpected intensification in the Gulf of Mexico that coincided with its encounter with a warm core ring (WCR). The relative positions of Opal and the WCR and the timing of the intensification indicate strong air–sea interactions between the tropical cyclone and the ocean. To study the mutual response of Opal and the Gulf of Mexico, a coupled model is used consisting of a nonhydrostatic atmospheric component of the Naval Research Laboratory's Coupled Ocean–Atmosphere Mesoscale Prediction System (COAMPS), and the hydrostatic Geophysical Fluid Dynamics Laboratory's Modular Ocean Model version 2 (MOM 2).

The coupling between the ocean and the atmosphere components of the model are accomplished by conservation of heat, salt, momentum, as well as the sensible and latent heat fluxes at the air–sea interface. The atmospheric model has two nests with spatial resolutions of 0.6° and 0.2°. The ocean model has a uniform resolution of 0.2°. The oceanic model domain covers the Gulf of Mexico basin and coincides with a fine-mesh atmospheric domain of the COAMPS. The initial condition for the atmospheric component of COAMPS is the archived Navy Operational Global Atmospheric Prediction System operational global analysis, enhanced with observations. The initial ocean condition for the oceanic component is obtained from a 2-yr MOM 2 simulation with climatological forcing and fixed mass inflow into the Gulf. The initial state in the Gulf of Mexico consists of a realistic Loop Current and a shed WCR.

The 72-h simulation of the coupled system starting from 1200 UTC 2 October 1995 reproduces the observed storm intensity with a minimum sea level pressure (MSLP) of 918 hPa, occurring at 1800 UTC 4 October, a 6-h delay compared to the observation. The rapid intensification to the maximum intensity and the subsequent weakening are not as dramatic as the observed. The simulated track is located slightly to the east of the observed track, placing it directly over the simulated WCR, where the sea surface temperature (SST) cooling is approximately 0.5°C, consistent with buoy measurements acquired within the WCR. This cooling is significantly less over the WCR than over the common Gulf water due to the deeper and warmer layers in the WCR. Wind-induced currents of 150 cm s^{-1} are similar to those in earlier idealized simulations, and the forced current field in Opal's wake is characterized by near-inertial oscillations superimposed on the anticyclonic circulation around the WCR.

Several numerical experiments are conducted to isolate the effects of the WCR and the ocean–atmosphere coupling. The major findings of these numerical experiments are summarized as follows.

1) Opal intensifies an additional 17 hPa between the times when Opal's center enters and exits the outer edge of the WCR. Without the WCR, Opal only intensifies another 7 hPa in the same period.
2) The maximum surface sensible and latent heat flux amounts to 2842 W m^{-2}. This occurs when Opal's surface circulation brings northwesterly flow over the SST gradient in the northwestern quadrant of the WCR.
3) Opal extracts 40% of the available heat capacity (temperature greater than 26°C) from the WCR.
4) While the WCR enhances the tropical cyclone and ocean coupling as indicated by strong interfacial fluxes, it reduces the negative feedback. The negative feedback of the induced SST cooling to Hurricane Opal is 5 hPa. This small feedback is due to the relatively large heat content of the WCR, and the negative feedback is stronger in the absence of the WCR, producing a difference of 8 hPa in the MSLP of Opal.

@ Current affiliation: University Corporation for Atmospheric Research/Naval Research Laboratory, Monterey, California.

Corresponding author address: Dr. Simon W. Chang, Naval Research Laboratory, Monterey, CA 93943.
E-mail: simon.chang@nrl.navy.mil

1. Introduction

It is well known that ocean supplies most of the energy for the development and intensification of tropical cyclones through interfacial transfers of heat fluxes. Tropical cyclones weaken quickly when cut off from these fluxes as they move into land or over cold ocean surface. The dependence of tropical cyclone on ocean conditions, especially the surface and subsurface temperature is well documented in many observational studies (Fisher 1958; Miller 1958; Tisdale and Clapp 1963; Leipper 1967; Perlroth 1967, 1969; Brand 1971; Namias 1976). Emanuel (1986) argues that the intensification and maintenance of tropical cyclones depend exclusively on the self-induced evaporation from the ocean without the constructive participation of ambient convective potential. Based on his assumption, the mature storm can be thought of as a simple Carnot engine, acquiring heat at the high-temperature ocean surface and losing heat near the low-temperature tropopause. The important thermodynamic interaction, even in the developing stage, is between the vortex and ocean with cumulus convection rapidly redistributing heat acquired at the oceanic source upward and outward to the upper-tropospheric sink.

Tropical cyclones can modify the mass and momentum fields of the ocean near their paths (Black 1983; Brooks 1983; Lai and Sanford 1986; Shay et al. 1992, 2000). The mechanical and thermal forcings exerted by tropical cyclones can spin up ocean circulations and reduce the surface and subsurface temperature, which may feedback to the overlaying storm, or remain as long-lasting wake to affect other systems that translate over it. The observed induced ocean response consists of a cold pool of surface temperature to the right of the storm track and a cyclonic near-surface current field associated with upwelling just behind the storm (Black 1983). In the wake, tropical cyclones typically leave a barotropic trough at the ocean surface (Shay et al. 1990) and a baroclinic ridge at the thermocline, accompanied by gradiently balanced currents with near-inertial oscillations (Shay et al. 1992, 1998).

In earlier numerical studies of the effect of the interaction of tropical cyclone and ocean (Chang and Anthes 1979; Anthes and Chang 1978), it was concluded that there is a negative feedback between the ocean and the tropical cyclone. This means that the cyclone-induced ocean response will act to weaken the tropical cyclone, and the weakened storm in turn will incur a reduced oceanic response. These conclusions were based on an axisymmetric, coupled model with coarse vertical resolution. The typical induced ocean cooling was approximately 3°C and the reduced minimum pressure, approximately 5 hPa. Recently, numerical studies with 3D coupled models (Sutyrin and Khain 1984; Bender et al. 1993; Ginis and Sutyrin 1995) have found the mutual response between tropical cyclones and the ocean to be nearly twice as strong as earlier findings. The differences can be attributed to the initial ocean mixed layer depth, the temperature lapse rate below the thermocline, and the horizontal resolution of the hurricane model that affects storm intensity. But it is only the magnitude, and not the nature of the response, that is in question. It is sufficient to say that the mutual response and negative feedback play an important role in the behavior of tropical atmosphere and the upper ocean.

Hurricane Opal of 1995 presents an excellent opportunity to study the interaction between a tropical cyclone and the upper ocean. Hurricane Opal experienced a sudden and unpredicted intensification 24 h before its landfall, which severely reduced the effectiveness of coastal evacuation procedure and, as a result, caused considerable damage along the Mississippi, Alabama, and Florida coasts (Marks et al. 1998). During the rapid deepening from 965 hPa (with maximum wind of 110 mph) to 916 hPa (130 mph) over 14 h, Opal moved over a warm core ring (WCR) that had separated from the Loop Current in the Gulf of Mexico (Fig. 1). During the same period, an upper-tropospheric westerly trough was approaching from the west to the northern Gulf of Mexico, which may have affected the intensification (Bosart et al. 2000).

The goal of this study is to analyze simulated interactions between Hurricane Opal and the WCR with a 3D coupled numerical model with a realistic initial condition. In earlier numerical studies with coupled models, either the atmospheric vortex representing the tropical cyclone or the initial ocean condition, or both the atmospheric and oceanic conditions, were oversimplified. Due to the lack of observations and reliable analyses, the initial condition for the ocean model was especially problematic. Several ocean models in coupled model studies use a climatic thermodynamic field at rest, which is not a realistic representative of the real ocean. An important aspect in this study is to obtain a reasonable representation of the atmospheric as well as the oceanic states during Opal. It is equally important to obtain a control simulation where the behavior of the tropical cyclone and the ocean is consistent with the observed properties prior to conducting extensive numerical experiments.

Accordingly, the paper is organized as follows. Section 2 presents a synoptic overview of Hurricane Opal and the Gulf of Mexico in early October of 1995. Section 3 gives a brief description of the atmospheric component and oceanic component of the coupled model, and the coupling mechanisms. Section 4 presents the initial conditions for the atmosphere and ocean models, and the experimental design of the study. The results will be presented in section 5, followed by a summary in section 6.

2. Synoptic overview of Hurricane Opal and the Gulf of Mexico in early October 1995

Hurricane Opal originated from a tropical wave that emerged from the west coast of Africa on 11 September

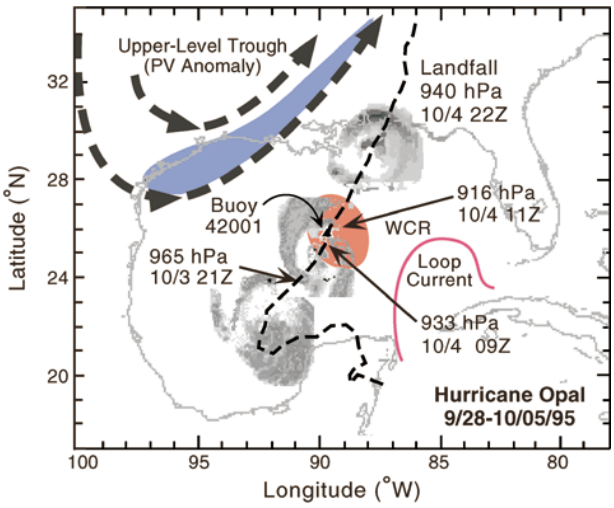

FIG. 1. Observed track of Hurricane Opal and locations of upper-level trough and the Loop Current warm core ring (WCR). Track (a bold dotted line) is from 28 Sep to 5 Oct 1995. The upper-level trough location at 1200 UTC 4 Oct (the bold dashed line) and the positive PV anomaly associated with the trough (the blue area) is derived from upper-level analyses. The WCR is derived from TOPEX altimeter data (the red area in the center of Gulf). The storm's internal structure is represented by SSM/I 85-Ghz imagery at 1629 UTC 3 Oct, 0337 UTC 4 Oct, and 1555 UTC 4 Oct. The 85-Ghz blackbody temperatures are depicted as shades of gray (adopted from Marks et al. 1998).

1995. The wave moved westward across the Atlantic into the western Caribbean Sea by 23 September and merged with a broad area of low pressure centered in the vicinity of 15°N, 80°W. The combined system drifted west-northwestward toward the Yucatan Peninsula over the following few days without significant development. Deep convection increased near the center of the low and a tropical depression formed about 125 km south-southeast of Cozumel, Mexico, at 1800 UTC 27 September.

Steering currents were generally weak and the tropical depression moved slowly over the Yucatan Peninsula for the following three days. Convective banding increased and the depression became Tropical Storm Opal at 1200 UTC 30 September while centered near the north-central coast of the Yucatan Peninsula. The storm gradually strengthened and moved slowly westward into the Bay of Campeche.

As its minimum central pressure steadily decreased, Tropical Storm Opal attained hurricane strength near 1200 UTC 2 October while centered about 270 km west of Merida, Mexico. A noticeable eye appeared in satellite imagery later in the day while a large-amplitude mid- to upper-level trough moved into the central United States. On 3 and 4 October, the hurricane turned toward the north-northeast and gradually accelerated to a speed of up to 8 m s^{-1}. During this period, the upper ocean's temperatures beneath the hurricane circulation were between 28° and 29°C, and a large upper-level anticyclone was well established over the Gulf of Mexico (Fig. 1). Rapid intensification ensued as evident by the reduction of the radius of the maximum wind R_{max} to 20–25 km, and was categorized as a category 4 hurricane on the Saffir–Simpson hurricane scale early on 4 October. The minimum central pressure of 916 hPa with the maximum sustained surface winds estimated at 65 m s^{-1} occurred when the hurricane was centered about 450 km south-southwest of Pensacola, Florida, at 1000 UTC 4 October. The peak intensity appears to have occurred near the end of an eyewall contraction cycle. Soon thereafter, the small inner eyewall diminished as an outer eyewall became more dominant. The hurricane weakened during this process, but was still a marginal category 3 hurricane as the center made landfall at Pensacola Beach near 2200 UTC 4 October.

The Advanced Very High Resolution Radiometer (AVHRR) derived sea surface temperatures (SSTs) were, in general, warmer than 29°C with no apparent organized structure in the Gulf of Mexico prior to the movement of Opal into the Gulf (Fig. 2). This situation was due to strong solar heating that occurs during the summer months, particularly June–September (Shay et al. 1992; Vukovich et al. 1979). The strong solar heating creates a thin layer of warm water, thereby masking the underlying features. However, as seen from the altimeter on board the National Aeronautics and Space Administration's Oceanographic Topography Experiment (TOPEX) mission, there was a warm ocean feature for TOPEX cycle 111 (18–27 September 1995) prior to the passage of Opal, located near 26.6°N and 87.5°W just to the east of the path. As detailed in Shay et al. (2000), the WCR had a maximum surface height anomaly (SHA) approaching 30 cm prior to the passage of Opal (Fig. 3a) with an SST of 29°C. Based on the mean translation speed of 3 to 4 km day^{-1}, the position of the WCR was located approximately at 26.5°N and 89°W on 1 October. After the passage of Opal, the maximum SHA associated with the WCR decreased by ~10 cm to approximately 20 cm (Fig. 3b) with cooling of about 0.5°C based on a National Data Buoy Center (NDBC) buoy 42001 located within the WCR and post-Opal AVHRR-derived SSTs. The net SST cooling of 2°–3°C was observed along the track prior and subsequent to encountering the WCR consistent with previous findings of Black (1983).

3. The coupled model

The Naval Research Laboratory (NRL) Coupled Ocean–Atmosphere Mesoscale Prediction System (COAMPS) and the Geophysical Fluid Dynamics Laboratory's (GFDL) Modular Ocean Model version 2 (MOM2) form the coupled system used in this study.

a. The atmospheric component

The COAMPS atmospheric model is based on nonhydrostatic, compressible dynamics of Klemp and Wil-

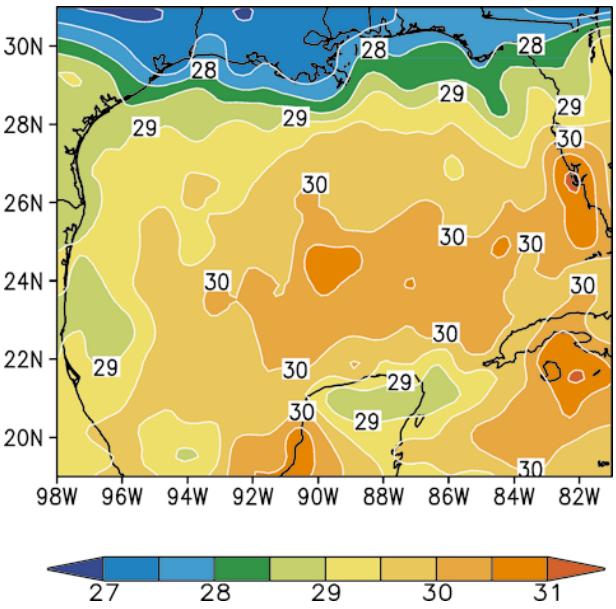

FIG. 2. Objectively analyzed AVHRR SSTs obtained from the COAMPS Ocean Data Assimilation (CODA) for 27 Sep 1995, which is the last date that images are unaffected by cloud over the Gulf of Mexico during Hurricane Opal.

helmson (1978). The parameterized physics include subgrid-scale mixing (Deardorff 1980), boundary and surface-layer formulation of Louis et al. (1982), explicit moist physics (Rutledge and Hobbs 1983) for grid-scale precipitation, cumulus parameterization of Kain (1990) and Kain and Fritsch (1993), and the radiative transfer of Harshvardan et al. (1987). A detailed description of the model can be found in Hodur (1997) and Xu (1995).

For this study, two-nested grids covering a domain from 0° to 54°N and from 121° to 39.4°W includes the tropical and midlatitude large environmental flow around Opal (Fig. 4). The outer coarse grid has 137 × 91 × 30 points with 0.6° longitude and latitude resolution horizontally. The inner, finer-scale grid has 247 × 136 × 30 points with 0.2° resolution with an inner grid domain extending from 9° to 36°N and from 98.2° to 49.0°W to encompass the immediate area covered by Opal's circulation. The vertical coordinate is in sigma *z* with 30 vertical levels in the model. The heights for any grid points over the ocean are 10, 30, 55, 90, 140, 215, 330, 500, . . . , m, etc.

Over land, surface albedo, surface roughness, and ground wetness are bilinearly interpolated to the model grids from monthly climatology. Over water, the albedo is set to 0.09 and the ground wetness is set to 1.0. The initial ground temperature is set to the initial lowest model temperature over land points. A surface energy balance equation is used to calculate the surface soil temperature. SSTs are prescribed from the Fleet Numerical Meteorology and Oceanography Center analyses based on Multi-Channel Sea Surface Temperature (MCSST) in uncoupled cases and from the ocean model

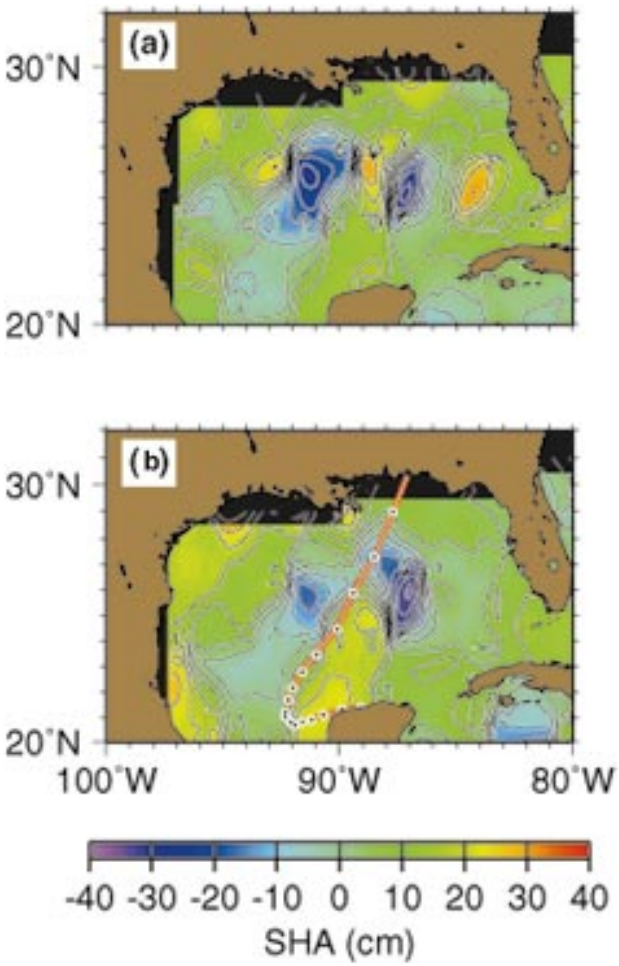

FIG. 3. (a) Prestorm (cycle 111, 18–27 Sep 1995) and (b) poststorm (cycle 112, 28 Sep–8 Oct 1995) altimeter-derived SHA map showing height anomalies corresponding to the WCE (from Shay et al. 2000).

in coupled cases. The surface terrain height is obtained from the U.S. Navy 20′ resolution terrain field.

b. The ocean component

The GFDL's MOM2 is a three-dimensional primitive equation ocean model (Bryan 1969; Semtner 1974; Cox 1984; Paconowski 1996). The governing equations consist of the Navier–Stokes equations using the Boussinesq, hydrostatic approximations. A nonlinear equation of state uses the temperature and salinity to calculate the ocean density. A free surface equation is solved for surface height perturbations.

The circulation in MOM2 is driven by interfacial fluxes of momentum, sensible and latent heat, and short- and longwave radiation. Vertical mixing is parameterized based on a Richardson number closure scheme (Pacanowski and Philander 1981). In this scheme, vertical mixing occurs when the Richardson number becomes subcritical ($R_i > 1$). The vertical mixing coefficients take the form of

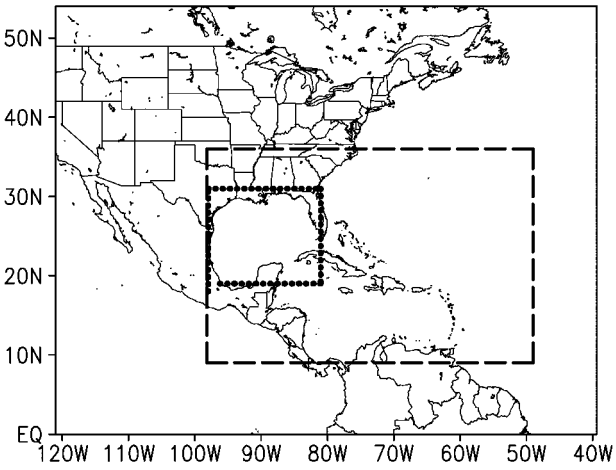

FIG. 4. The atmospheric model domains for coarse- and fine-mesh grids. The outer grid has 137 × 91 × 30 grid points with 0.6° resolution in both the *x* and *y* directions. The inner grid has 247 × 136 × 30 grid points with 0.2° resolution in both the *x* and *y* directions. The dotted box is a domain for the diagnosis. The oceanic domain and resolution is the same as the atmospheric fine-mesh grid.

$$K_h = \frac{c_1}{(1 + 5R_i)^3} + d_1 \quad \text{and} \tag{1}$$

$$K_m = \frac{c_1}{(1 + 5R_i)^2} + \upsilon_1, \tag{2}$$

where R_i is the gradient Richardson number, d_1 is a background diffusion coefficient, and υ_1 is the viscosity coefficient. Reasonable values for the maximum mixing coefficient c_1 range from about 50 to 100 cm^2 s^{-1}. Supplementary sensitivity tests have been carried out in an attempt to obtain the observed surface cooling. We found that the observed cooling is not approached until the value of c_1 is set at 1000 cm^2 s^{-1}. Beyond this value, however, no additional cooling can be achieved. Therefore a value of 1000 cm^2 s^{-1} is used for c_1. The coefficient d_1 varies from molecular values of 0.001 34 cm^2 s^{-1} to bulk values of about 0.1 cm^2 s^{-1}, and υ_1 varies from molecular values of 0.0134 cm^2 s^{-1} to bulk values of about 1.0 cm^2 s^{-1}. In the case $R_i < 0$, the vertical mixing coefficients default to 10^6 cm^2 s^{-1}.

A staggered B grid is used with the vertical coordinate in depth *z*. The Scripps 1° bathymetry is interpolated to the oceanic grid. For our study, 20 vertical levels are set up in MOM2, where the depths are 5, 17, 36, 67, 113, 179, 267, 381, 522, 692, 892, . . . , m, etc. A finer vertical resolution near the surface may relax the requirement of the large value used for c_1, but the available computing resources limit our choices.

The initial ocean conditions that realistically describes the Gulf of Mexico prior to Opal are difficult to obtain. In view of the lack of subsurface observations and a global ocean analysis, it is necessary to integrate the MOM2 globally at a horizontal resolution of 1° lat × 2° long to obtain the commonly observed boundary and gap flows, including the Gulf of Mexico Loop Current and the Florida Current. Initial temperature and salinity fields for this global simulation are the monthly Levitus (1982) climatology for October. The surface boundary conditions including surface wind stress and heat fluxes at the ocean surface are derived from Esbensen and Kushnir's (1981) global ocean heat budget. Heat fluxes are composed of latent, sensible, and longwave and solar shortwave components. The solar short wave is allowed to penetrate to subsurface layers to avoid overheating in the first ocean model layer. After a 2-yr model integration, a reasonable, quasi-steady-state global ocean circulation appropriate for the horizontal resolution is achieved in the ocean model domain.

A limited-area MOM2 is set up with a horizontal resolution of 0.2° longitude and latitude to further resolve more oceanic structure in the Gulf of Mexico (Fig. 4). The limited-area MOM2 has the same domain as the inner grid of COAMPS extending to the mid–Atlantic Ridge to provide representative conditions for shears, temperatures, and salinities for the inflow conditions (Sturges et al. 1993). Similar to the global simulation, a 2-yr simulation with the limited-area MOM2 is conducted using the same climatological initial conditions and surface forcing. To maintain the model consistency, the results of the global 2-yr MOM2 simulation are used as the boundary conditions for the 2-yr integration of the limited-area MOM2.

A flow relaxation scheme of Davies (1976, 1983), similar to that in the COAMPS atmospheric component, is used to introduce the global MOM2 fields into the limited-area MOM2 (Martinsen and Engedahl 1987). Thus, except for the constant boundary conditions, the limited-area MOM2 acts like an inner grid to the global MOM2 in a one-way nesting. In all the simulations, the air–sea coupling occurs only over the limited-area MOM2 domain.

c. Coupling mechanisms

The coupling of the atmospheric and the oceanic components is based on the conservation of momentum, sensible heat, latent heat, and mass fluxes through the air–sea interface. The surface frictional velocity (u_*), temperature (θ_*), and humidity (q_*) used in the estimates of fluxes (Louis et al. 1982) are computed across the interface as

$$u_* = \left[u^2 f_m\left(\frac{z}{z_0}, R_i\right)\right]^{(1/2)},$$

where

$$u = \sqrt{(u_a - u_o)^2 + (v_a - v_o)^2}, \quad (3)$$

$$\theta_* = \frac{u(\theta_o - \theta_a) f_h\left(\frac{z}{z_0}, R_i\right)}{r u_*}, \quad \text{and} \quad (4)$$

$$q_* = \frac{u(q_{vo} - q_{va}) f_h\left(\frac{z}{z_0}, R_i\right)}{(r u_*)}, \quad (5)$$

where subscript a denotes quantities at the lowest model level in the atmosphere ($\sim$10 m) and subscript o represents quantities at the uppermost ocean level (~ -2.5 m); f_m and f_h are stability functions of gradient Richardson number R_i and surface roughness z_o, which is estimated from the Charnock's equation. The latent heat for evaporation is assumed to be extracted from the ocean surface layer, and the precipitation contributes to the ocean as a salinity sink and a freshwater source at the same temperature as the SST. These exchanges across the air–sea interface can occur either at each atmosphere or at each ocean model time step. When coupling at each ocean model time step, the fluxes of heat, moisture, momentum, and total precipitation are averaged over all atmospheric time steps during one ocean time step. Upper-level temperatures of the oceanic component are fixed as the SSTs during all atmospheric time steps within any one ocean time step.

In the coupled model, the time step of inner atmospheric grid is three times smaller than that used in the coarse atmospheric grid, which equals the time step of the limited-area ocean model. Thus, fluxes of heat, moisture, momentum, and mass from the atmospheric are summed over three time steps of the inner atmospheric grid before exchanges occur with the upper ocean. During the three time steps, the ocean conditions are held constant for the flux calculations.

4. Initial conditions at 1200 UTC 2 October 1995

a. The initial atmospheric conditions

The first-guess fields for the initial condition are obtained from the Navy Operational Global Atmosphere Prediction System (NOGAPS) analysis valid for 1200 UTC 2 October 1995. In the NOGAPS analysis, a bogus vortex (Goerss and Jeffries 1994; Goerss et al. 1998) representing the inner circulation of Opal is introduced to represent Opal on the NOGAPS grid. The first-guess fields are reanalyzed for COAMPS grids by a multivariate optimum interpolation (MVOI) analysis technique (Lorenc 1986). In MVOI, a volumetric method is applied to construct separate analyses for each nested grid with available observations in the domain on 16 mandatory pressure levels from 1000 to 10 hPa. The wind observations are obtained from rawinsondes, pibals, AIREPS, the Aircraft Communications Addressing and Reporting System, Special Sensor Microwave/Imager (SSM/I), surface, and cloud-tracked winds. Heights and thicknesses are obtained from rawinsondes, and Defense Meteorological Satellite Program and National Oceanic and Atmospheric Administration satellite retrievals. Initial fields with different bogus vortex have been tested. While different initial vortices resulted in different intensifications, there are no discernible simple relationships between the initial and the maximum intensities of these systems. Boundary conditions for the prognostic fields are supplied to the coarse mesh at 12-h intervals from NOGAPS analyses. The lateral boundary treatment of Davies (1976, 1983) is used to blend the NOGAPS analyses and the COAMPS predicted fields.

b. The initial ocean conditions

The initial ocean fields are obtained from a 690-day simulation of the Gulf of Mexico with climatological forcing (Esbensen and Kushnir 1981) and a fixed boundary condition from the 2-yr global MOM2 simulation as shown in Fig. 5. The prominent features shown in Fig. 5 are the anticyclonically rotating WCR shed from the Loop Current. The WCR is located at 25°N and 89°W, which is about 1° latitude south of the altimeter-derived WCR location (Shay et al. 2000). The maximum height anomalies of 40 cm is $\sim$10 cm higher than that referred from TOPEX (Fig. 3a). The maximum current speed of 75 cm s^{-1} associated with the WCR is consistent with previous observations in the case of Gilbert (Shay et al. 1992, 1998).

The simulated SST is 2°–3°C cooler as compared with the objectively analyzed SST field from AVHRR (Fig. 2) valid for 27 September 1995, which is the last date prior to Opal's passage after which the retrieval is affected by cloud cover over the Gulf of Mexico. This cooler SST is a systematic bias of MOM2 with the climatological forcing over this region. Another major difference between the SST fields is the absence of the cold SST pattern in the eastern Gulf of Mexico in the SST analysis based on the AVHRR retrieval. There is a 4°C SST difference in the simulation as compared to a 2°C in the AVHRR-derived SST. This cold water represents the filamentation process where streamers of colder west Florida shelf water are entrained into the loop current and WCR, which has been realistically reproduced by MOM2. The physical effect compares well with the analysis of Vukovich and Maul (1985).

There are no in situ profile measurements in the Gulf of Mexico prior to the passage of Hurricane Opal. The simulated temperature and salinity profiles in the WCR and in the common Gulf water are compared with those taken prior to Hurricane Gilbert of 1988 (Fig. 6). This comparison is by no means a validation; rather, this comparison is made to ensure the simulated vertical structure is within bounds at least in a qualitative sense. As shown in Fig. 6a, the simulated temperature of the common water is about 1.5°–2°C warmer than the com-

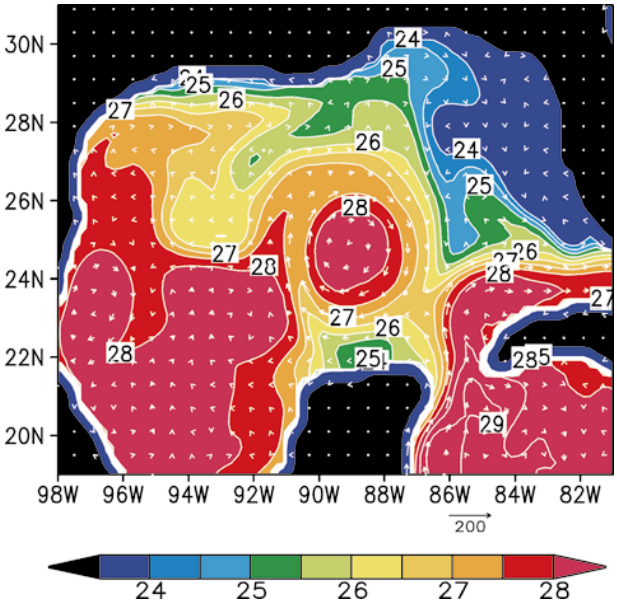

FIG. 5. Sea surface temperature (contours) and current speed (vectors in cm s^{-1}) obtained from a 690-day simulation in the Gulf of Mexico basin.

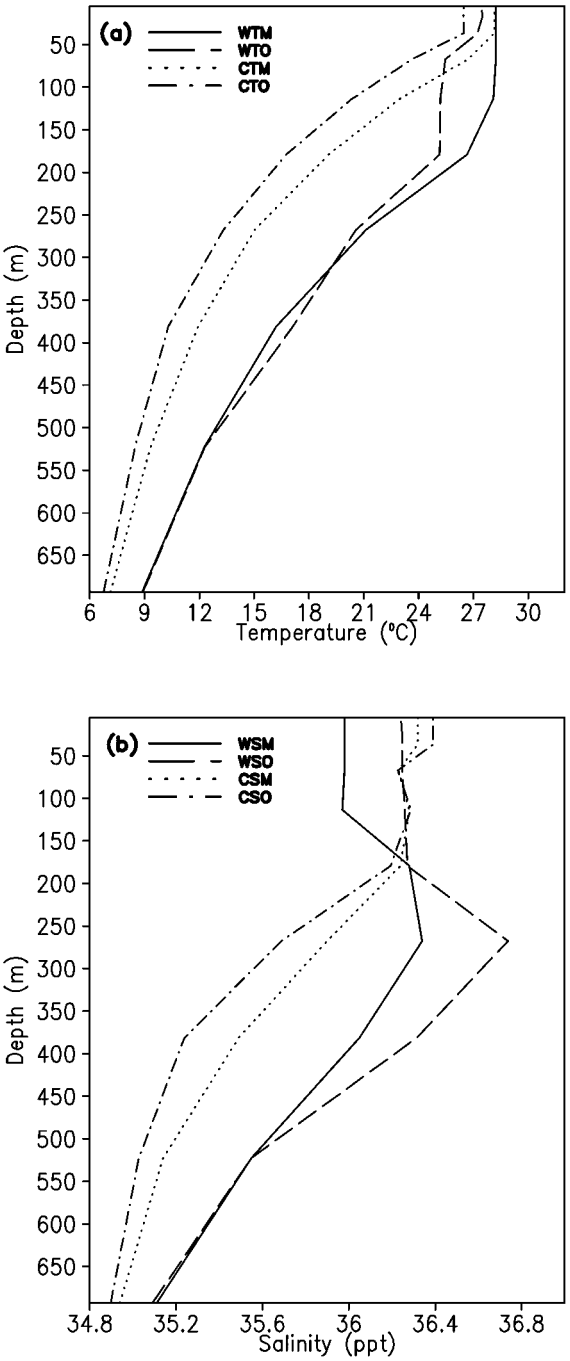

FIG. 6. Vertical profiles of (a) temperature and (b) salinity from the observations and from the model simulations. The letters W, C, T, S, M, and O in the figure represent the warm core ring, common water, temperature, salinity, model output, and observed, respectively. The initial time of the coupled model simulation (t1) is 1200 UTC 2 Oct 1995. The locations of the simulated WCR and the common water are at (25°N, 89°W) and the location for common water is chosen at (23°N, 91.5°W).

mon Gulf water in 1988. The simulated temperature profile in the WCR is similar to one observed in a WCR prior to Hurricane Gilbert below 200-m depth (Shay et al. 1998). Above 200 m, the simulated WCR is warmer. Observed and simulated temperature profiles have similar vertical gradients—an important characteristic for cooling due to shear-induced vertical mixing events and volume transports as noted in Price (1981). It is also interesting to note that the WCR is identifiable down to at least 700 m because of combined barotropic and baroclinic components.

The simulated salinity profile in the common Gulf water is similar to the representative profile (Fig. 6b). The simulated salinity decreases with depth in the common water, whereas the salinity increases with depth to the depth of 200–300 m in the WCR and then decreases with depth below 300 m. In addition, the WCR is less saline than the common water from the surface to a depth of 200 m. The model produces less saline water above the 500-m depth in the WCR by 0.4 ppt as compared to the observed profile.

c. Experimental design

As listed in Table 1, the first five numerical experiments start from 1200 UTC 2 October 1995 and continue for 72 h. In the first experiment (expt C1), the atmospheric and oceanic components are fully coupled. In the second experiment (expt U1), the ocean is held constant at its initial state, where the initial SST from the MOM2 spinup is 2° to 3°C cooler than the MCSST. For consistency, a surface temperature of 2.5°C is arbitrarily added everywhere in the MOM2 spinup ocean

TABLE 1. List of numerical experiments.

Expt	Coupling	Atmosphere	Ocean
C1	Coupled	With Opal	With WCR
U1	Uncoupled	With Opal	Fixed with WCR
C2	Coupled	With Opal	With no WCR
U2	Uncoupled	With Opal	Fixed with no WCR
MCSST	Uncoupled	With Opal	Fixed MCSST
O	Uncoupled	Climatology	With WCR
O1	Uncoupled	No forcing after Opal's landfall	With WCR

initial conditions. Thus, the mean SST in the initial state is the same as the mean MCSST-based SST analysis.

To further isolate the effect of the WCR, two sensitivity experiments are conducted without the presence of the WCR. There are several ways to create an initial ocean state without the WCR. We select the simplest: replacing the thermodynamic fields of the WCR within a radius of 2.5° lat with the property of the common water and setting the current to zero. We found that the WCR can be completely replaced with little changes outside the WCR and no noticeable imbalance anywhere in the model. Numerical integration is carried out to check the adjustment after the removal of the density gradients and the adjustment is minimal. A coupled (expt C2) and an uncoupled (expt U2) experiments are then conducted based on this ocean initial condition with no WCR.

Three additional baseline integrations are also conducted for detailed comparisons between the various simulations. In experiment MCSST, the atmospheric component is integrated in an uncoupled mode with the MCSST valid for 27 September 1995 (Fig. 3). In experiment O, the ocean component is integrated for 72 h with climatological forcing. The ocean condition changes little in experiment O except for some westward drift of the WCR, consistent with previous studies. Experiment O1 is a continuation of experiment C1 after 1200 UTC 5 October 1995 where the ocean component is integrated without atmospheric forcing. Experiment O1 is integrated for one month to check the restoring forces within the WCR subjected to such strong forcing.

5. Results

Numerical results presented in this section are organized into the evolution of Opal, the hurricane-induced response, the effect of the WCR on Opal, the effect of Opal on the WCR, and the net effect of the coupling and feedback.

a. Evolution of Opal's intensity

As shown in Fig. 7, observed and simulated tracks of Hurricane Opal in experiments C1 and C2 are superposed on the initial model SST (shaded) and surface height (contour) in the Gulf of Mexico. The observed

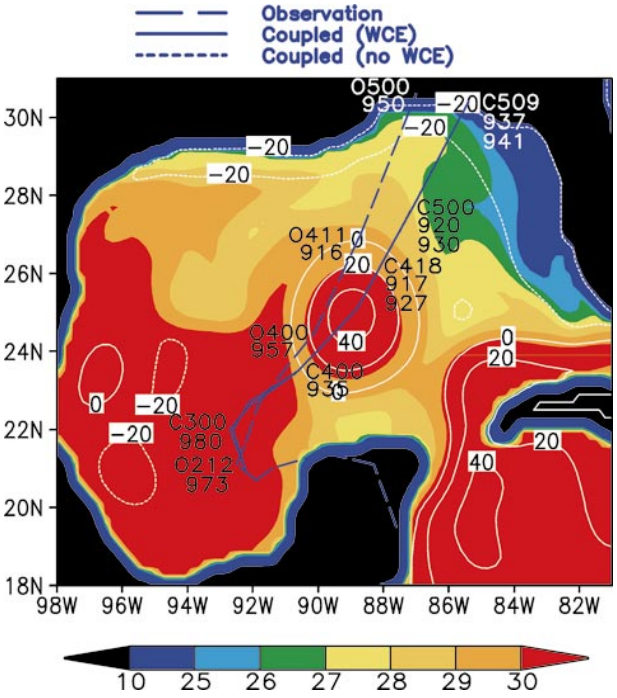

FIG. 7. Observed and simulated tracks of Hurricane Opal in expts C1 and U1 superimposed on the initial model SST (shaded) and surface height (contour) in the Gulf of Mexico. The letters O and M, followed by time (i.e., 212 gives the time 2 Oct 1200 UTC), represent the observed and model output, respectively. The letters C and U represent expts C1 and U1, respectively. The numbers in the second and third lines represent the minimum sea level pressure.

and simulated minimum central sea level pressures (MSLP) over the period of 72 h are given in Fig. 8.

The simulated track is located to the east of the observed, passing right through the central point of the WCR. The simulated storm moves at a slower speed. The simulated time of landfall is 11 h after the observed landfall. At 72 h, the position error is approximately 440 km, within the normal range of operational numerical prediction of tropical cyclones (J. S. Goerss 1998, personal communications).

The evolution of Opal's minimum MSLP follows the general trend of the observed—rapid deepening followed by rapid weakening centered around the time of its encountering with the WCR—but differs in details. First, the observed minimum MSLP of Opal has a relatively steady MSLP near 970 hPa for about 24 h before undergoing rapid intensification during the second 24-h period during the window of interest. The maximum intensification of 41 hPa to 916 hPa occurred during an 11-h period from 0000 to 1100 UTC 4 October, upon encountering the WCR. By contrast, the intensification of the simulated Opal is much smoother. That is, the MSLP starts from 985 hPa, which is 12 hPa higher than the observed due to the coarse resolution of the global analysis, and deepens to 917 hPa around 1800 UTC 4 October. The delay in reaching the maximum intensity of approximately 7 h and the subsequent weakening

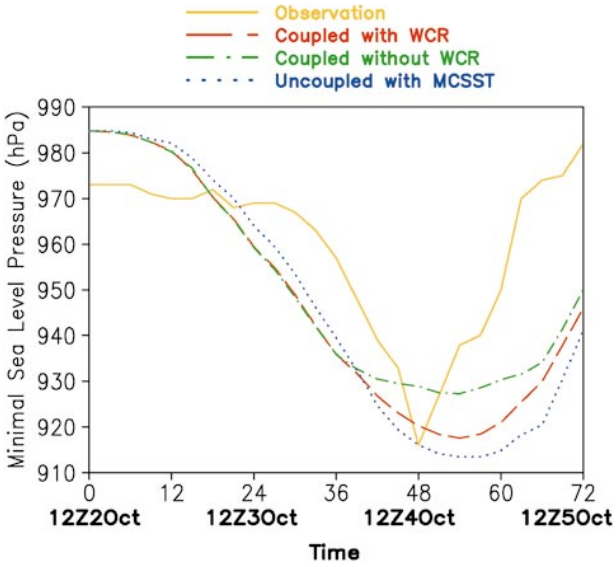

FIG. 8. Observed and simulated minimum sea level pressures from expts C1, U1, and MCSST over the period of 72 h.

(due to cooler SST and landfall) is related to the slower translation speed of about 7 m s^{-1} in the simulation compared to the observed translation speed of 8.5 m s^{-1}. After 66 h, the simulated weakening rate as the storm moves over the cold SST over the western Florida shelf is comparable to the observed averaged weakening after 1200 UTC 4 October.

It is interesting to note that the observed and simulated Opal reaches its maximum intensity as its center moves over and exits the WCR, outlined by the zero SHA contour (Fig. 7). Even though the timing of the event is shifted from the observed time, the simulated deepening (between 24 and 42 h) and weakening (66–72 h) rates are similar to that observed during Opal's passage. This leads us to believe that the relatively poor resolution of 20 km in COAMPS inner grid contributes to the smoothness of the pressure tendency.

b. Opal-induced oceanic response

The Gulf of Mexico is modified by the forcing of Opal both dynamically and thermodynamically.

1) THE DYNAMIC RESPONSE

As shown in observational and model studies (e.g., Chang and Anthes 1978; Price 1981; Black 1983; Shay et al. 1990), the typical dynamic response of the ocean to a passing tropical cyclone is characterized as a cyclonic, near-surface, spunup current field slightly beginning just in back of the eye. In this wake regime, mixed layer currents rotate near inertially with an alternating divergence and convergence pattern separated by approximately one inertial period, which induces upwelling and downwelling of the thermocline principally along the track. The presence of the near-surface currents in the wake is biased to the right side of the storm track due to the near synchronicity of the wind stress and mixed layer current. This stronger near-inertial current on the right side of the storm contains considerable vertical structure and large current shears across the base of the mixed layer as found in the Gilbert current profiles (Shay et al. 1998). The strong shears affect the thermal response of the ocean by lowering the Richardson numbers to below criticality that induces vertical mixing and cools the upper ocean (Jacob et al. 2000). The heat and mass budgets in the upper ocean are also modified by the preexisting horizontal inhomogenieties in the ocean as in the case of Opal and Gilbert.

At 1200 UTC 3 October, the induced cyclonic current field, with speed maxima over the continental shelf to the southwest (or right side) of the storm, starts to link with the WCR circulation (Fig. 9a). At 0000 UTC 4 October (Fig. 9b), as Opal begins to encounter the WCR, the southeast current located at the southwest quadrant of the WCR is accelerated to above 140 cm s^{-1}. Another current maximum is located to the rear of the storm, as the wind stress exerted by Opal tries to force the flow between the WCR and Yucatan over the Campeche Bank. The simulated Opal track is almost directly overlying the WCR at 1200 UTC 4 October. Under the cyclonically rotating wind stress, the anticyclonic current of the western section of the WCR is reduced (Fig. 9c), and the apparent oceanic circulation over the eastern portion of the WCR becomes *cyclonic*. The maximum speed is about 120 cm s^{-1}, weaker than the 140 cm s^{-1} that occurred earlier, located about 130 km to the right of the storm track. In fact, the SHA field of the WCR now appears asymmetric and distorted. The flow between the WCR and the Yucatan over the Campeche Bank reaches its maximum strength, connecting and widening the Loop Current. There is a maximum alongshore current of over 100 cm s^{-1} and the SHA increases to more than 20 cm along the northern edge of Yucatan due to the channeling of the flow. To the southwest of WCR, the hurricane-induced current field becomes anticyclonic, exhibiting the effect of the strong near-inertial oscillation in the wake of Opal.

As Opal moves past the WCR at 0000 UTC 5 October (Fig. 9d), the maximum current speed is accelerated to 200 cm s^{-1} located to the east of the WCR between the cyclonic and anticyclonic pattern. The SHA of the WCR is reduced to 10 cm, a 30-cm reduction from the prestorm height of 40 cm due to the integrated Ekman divergence associated with the barotropic trough and the loss of heat. The strong, predominant northerly surface currents over the southern and eastern WCR have distorted the WCR's SHA field with a longer axis in the southeast to northwest direction. As Opal moves farther north and makes landfall (Fig. 9e), the near-inertial oscillation in the wake weakens, the maximum SHA is restored to 30 cm and the induced asymmetry lessens. This 10-cm net reduction of SHA associated with the

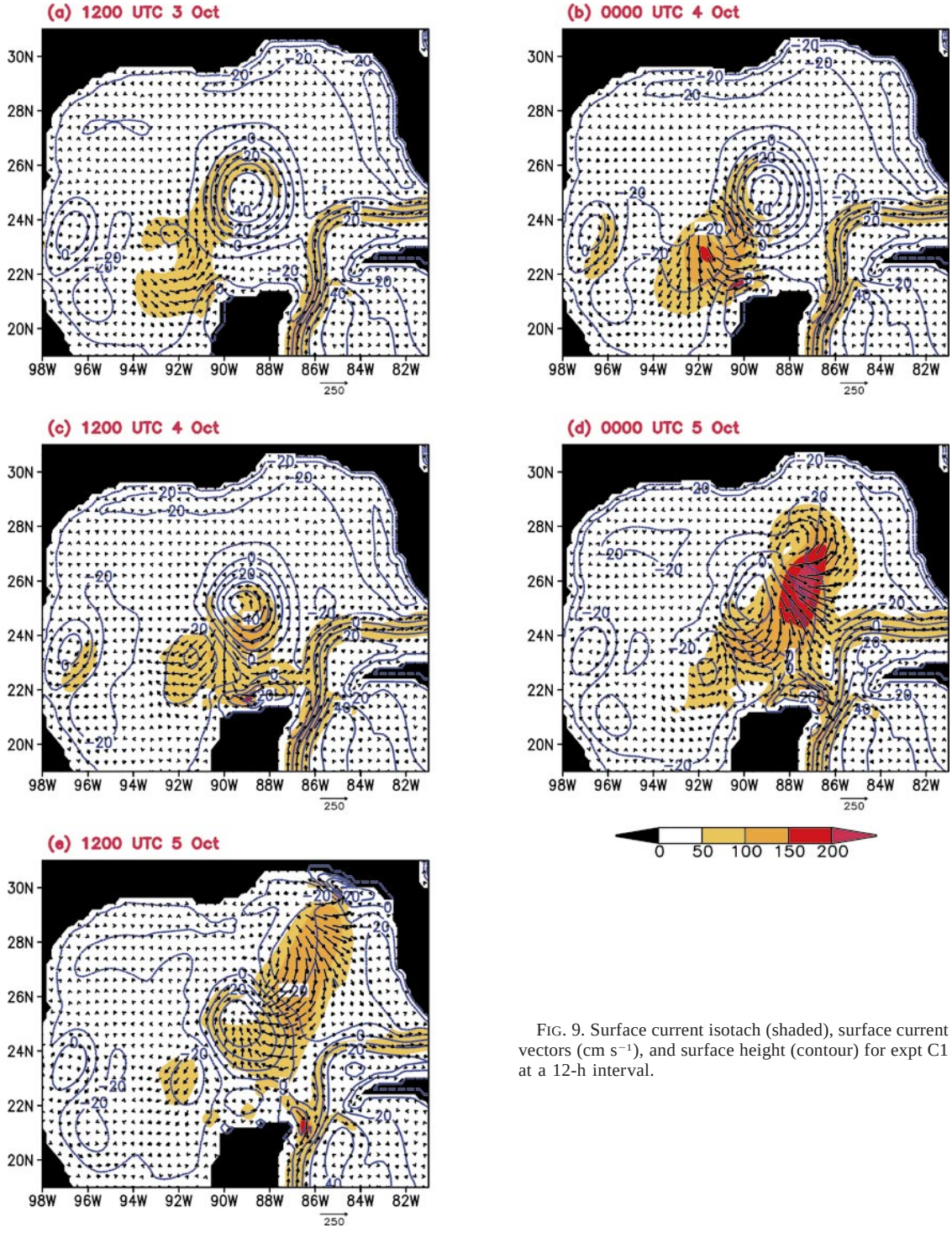

FIG. 9. Surface current isotach (shaded), surface current vectors (cm s^{-1}), and surface height (contour) for expt C1 at a 12-h interval.

WCR is in good agreement with the TOPEX altimeter-observed reduction (Fig. 3, or Shay et al. 2000). There is a long swath with storm-induced ocean current well over 100 cm s^{-1} to the right of the storm track between the WCR and the Florida panhandle, similar to earlier numerical studies with horizontally homogeneous initial ocean fields (e.g., Chang and Anthes 1979; Price 1981; Shay et al. 1990).

Continuing the integration of the ocean component after 1200 UTC 5 October without atmospheric forcing (expt O1), the shape and the strength of the WCR, indicated by the maximum SHA, never fully recover to

the prestorm condition. At the end of 30 days, the maximum SHA is approximately 75% of the prestorm value. In an idealized case, Shay et al. (1990) found the magnitude of the persistent barotropic trough in the wake of hurricanes is on the order of 10–20 cm, consistent with the result here.

2) THE THERMODYNAMIC RESPONSE

The SST and salinity changes induced by Opal are depicted in Fig. 10. In early numerical simulations with initially homogeneous ocean, the induced cool pool is in an elongated pattern located on the right side of the storm track, centered at approximately 2 R_{max}. Here, the distribution of the SST changes is modulated by the WCR. As shown in Fig. 10, the maximum cooling of 2.4°C is located to the southwest of the WCR, where the initial mixed layer is shallower (<50 m) with stronger stratification below the mixed layer. Over the WCR, the induced cooling is 0.46°C, due to the 200-m deep isothermal layer and a stronger stratification below (Fig. 6), which is consistent with the buoy measurements of 0.5°C during Opal (Shay et al. 2000). Even though Opal is much stronger after passing over the WCR, the cooling depends very much on the prestorm thermal structure based upon Richardson number argument. There is some correspondence of the salinity change to SST change—the salinity is generally reduced by the induced upwelling and by the introduction of freshwater from Opal's precipitation. However, there is very little salinity change over the WCR.

Pre- and poststorm vertical temperature and salinity profiles inside and outside the WCR are compared in Fig. 11. Figure 11a shows that the temperature profile in the WCR, having deeper and warmer layers, is cooled by about 0.5°C at the surface. In contrast, the cooling in the common water with shallow mixed layer is more than 2°C. Notice that the cooling at the 200-m level in the WCR is greater, due to the stronger upwelling induced by a stronger Opal as compared to the common water profile sampled at a lower latitude.

The effect of Opal on the salinity profile (Fig. 11b) is a net decrease of salinity almost everywhere in the common water due to upwelling and precipitation. For the WCR, the net effect is a small decrease in the surface, small increase above the depth of 260 m and a decrease below the depth of the 260 m as one would expect from the initial salinity profile.

c. The effect of the WCR on Opal

To further isolate the effect of the WCR on the behavior of Opal, experiment C2, a coupled experiment with an ocean initial condition otherwise identical to experiment C1 except without the WCR, is conducted. The generation of such ocean initial condition has been discussed in section 4.

As shown in Fig. 7, the track of Opal does not appear to be affected by the absence (or presence) of the WCR. The minimum central SLP of Opal is, however, considerably affected by the WCR. In both experiments C1 and C2 (Fig. 12), the minimum SLP deepens nearly identically from the initial value of 985 hPa at 1200 UTC 2 October to 934 hPa 36 h later at 0000 UTC 4 October. Subsequently as the center of Opal encounters the WCR regime, the two experiments differ markedly. Opal in experiment C1 continues to intensify by 17 hPa over the next 18 h, reaching a minimum central MSLP of 917 hPa. In the absence of the WCR in experiment C2, Opal decelerates its intensification phase after 0000

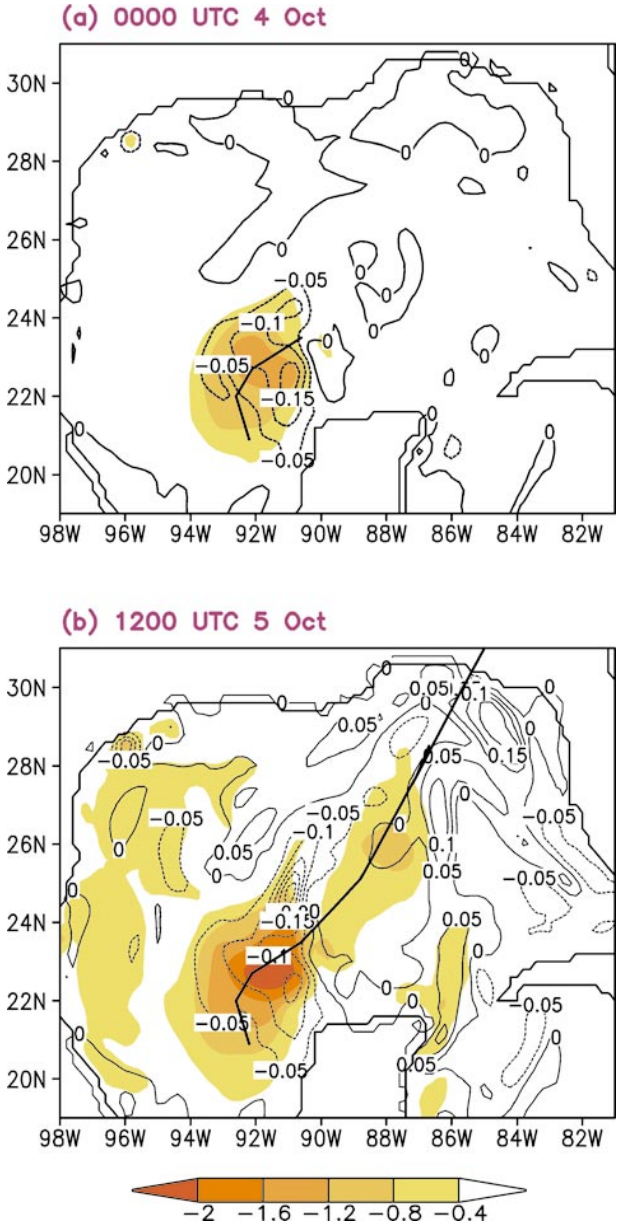

FIG. 10. Changes of the sea surface temperature (shaded) and the sea surface salinity (contours) at (a) 0000 UTC 4 Oct and (b) 1200 UTC 5 Oct for expt C1.

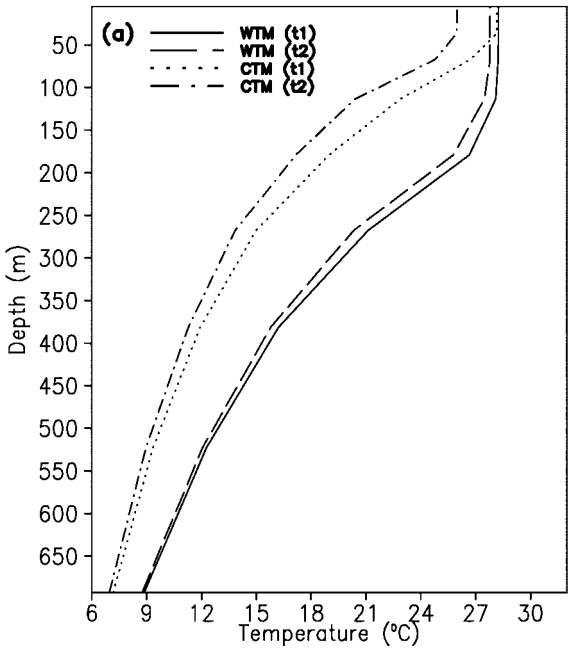

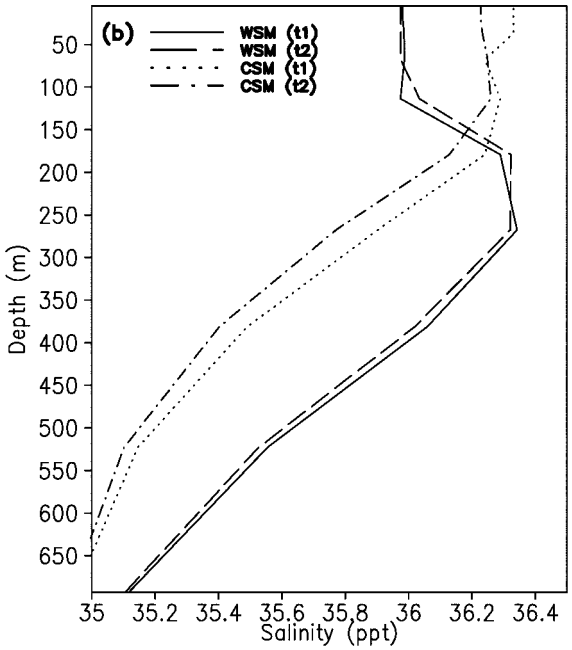

FIG. 11. Vertical profiles of (a) temperature and (b) salinity at 25°N, 89°W WCR and at 23°N, 91.5°W (common water) for 1200 UTC 2 Oct (t1) and for 1200 UTC 5 Oct (t2). The meanings of letters are the same as in Fig. 6.

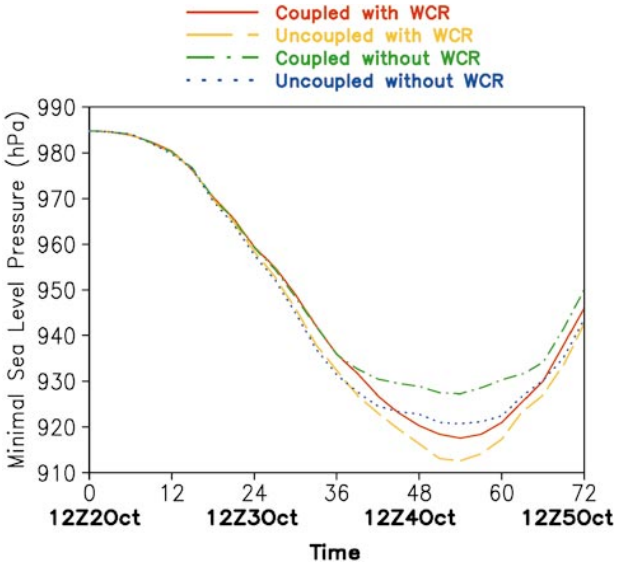

FIG. 12. Minimum sea level pressures from expts C1, U1, C2, and U2 over the period of 72 h.

UTC 4 October; its central pressure decreases only another 7 hPa to 927 hPa. Based upon these simulated results and agreement with observed changes in the atmosphere and the ocean, *the WCR is responsible for 60% of the final intensification of Opal.*

The MSLP, surface wind vectors, and the total accumulated 1-h precipitation for experiments C1 and C2 as Opal is exiting the northeastern edge of the WCR at 1800 UTC 4 October are shown in Fig. 13. As expected, the stronger total surface heat flux, both sensible and latent, from the WCR supports a stronger precipitation in C1 as compared to C2. On average, over 90% of the total precipitation are of the grid-scale precipitation, especially along the northern semicircle where strong precipitation occurs, and less than 10% are convective. Stronger precipitation in C1 results in a more intense tropical cyclone in C1. The effect of the WCR is also evident in the structure of the inner core represented by the equivalent potential temperature (EPT), as a measure of moist static energy, and the wind velocity component tangential to the cross section through the storm center. The EPT is high above the tropopause and in the inner core region. In Opal's outer circulation, the EPT increases with height except in the boundary layer, where the EPT is dominated by humidity, which decreases with height (figure not shown). In the inner region from experiment C1, the EPT is 370 K at the 450-hPa level, and 365 K at 600 hPa, and the EPT of the entire eye region is above 360 K. Estimates of the EPT from NDBC buoy 42001 range from 360 to 365 K at 10-m height in Opal's eyewall (Shay et al. 2000). Thus, there appears to be consistency between the simulated and observed EPT in the WCR. In experiment C2, these contours occur at higher altitudes at 200, 500, and 700 hPa, respectively. The EPT in the inner core is at least 3 K cooler than that in C1 below the 500-hPa level. The difference indicates there is less convective activity and a less intense atmosphere warm core in Opal in experiment C2 as compared to C1. This also suggests that the central convective region of C1 is more concentrated

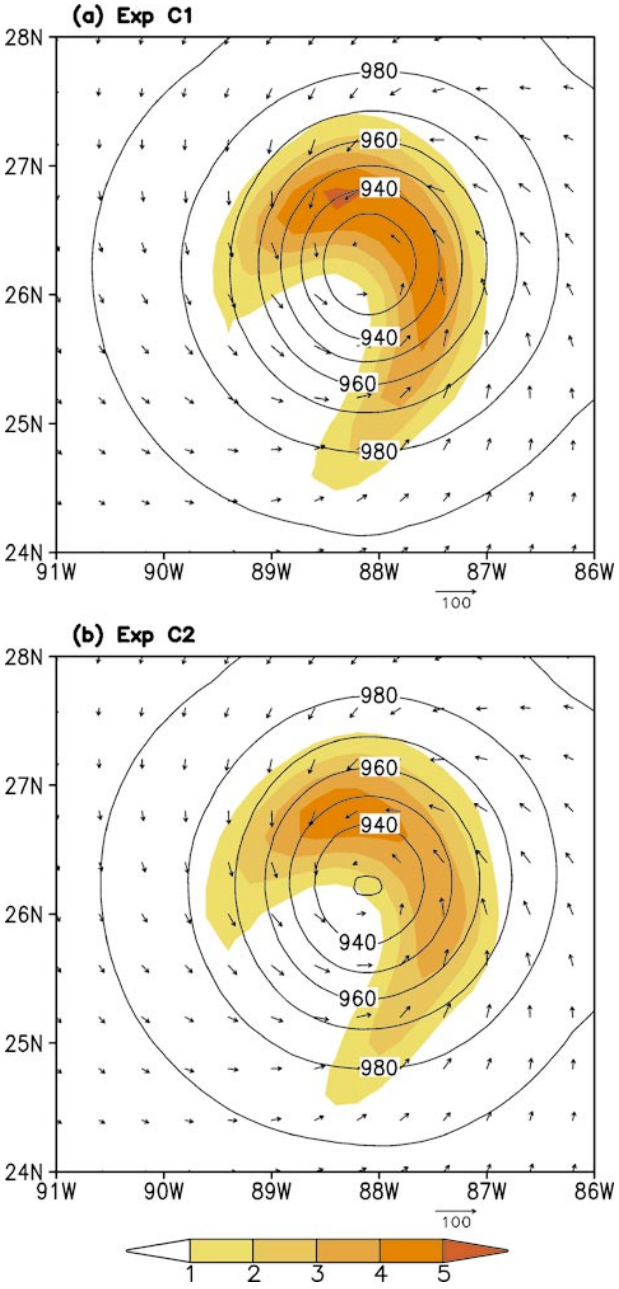

FIG. 13. Minimum sea level pressure (hPa), surface wind vectors (m s^{-1}), and the total 1-h accumulated precipitation from expts C1 and C2 at 1800 UTC 4 Oct.

than that in C2. All these results show that the tropical cyclone in C1 is more active, robust, and intense.

d. The effect of Opal on the WCR

Considerable differences in intensity and structure of the simulated Opal storm in experiments C1 and C2 are due in part to the large heat content of the WCR, which supports the sensible and especially the latent heat transfers to Opal. The heat content Q at a point is computed as

$$Q = \rho c_p \Delta T \Delta z, \tag{6}$$

where ρ is the oceanic density taken as 1 gm cm^{-3}, c_p is specific heat at constant pressure taken as 1 cal (g $K)^{-1}$, ΔT is the maximum of zero or the difference of ocean temperature and 26°C, and Δz is the maximum of zero or the depth of the 26°C isotherm. Ocean temperature warmer than 26°C is considered beneficial for the intensification of tropical cyclones (DeMaria and Kaplan 1994). The prestorm depth of the 26°C isotherm in the WCR is 180 m in experiment C1 and 60 m in the common water or in experiment C2 (figures not shown). Because of the warmer and deeper upper layer, Q at a selected point (25°N, 89°W) in the prestorm WCR in experiment C1 is 43 kcal cm^{-2} as compared to 10 kcal cm^{-2} in the common water. The relationship of the heat content of the WCR to the surface sensible and latent heat fluxes is illustrated by Figs. 14 and 15. At 0000 UTC 4 October as Opal just begins to encounter the WCR in experiment C1, the maximum heat content of the WCR is 45 units (10^3 cal cm^{-2}) at the center of the WCR (Fig. 14a). The total surface flux is closely correlated to the surface wind field with maxima in the range of 1500–2000 W m^{-2}. At 1800 UTC as Opal begins to exit the WCR, the maximum flux is increased to nearly 2842 W m^{-2} (Fig. 14b). The maximum heat content has thus decreased to 27 units at 0000 UTC 5 October. This equates to a difference of 18 units over an approximate period of 14 h. The rate of heat loss is then 15 kW m^{-2}, and given the heat flux of about 2600 W m^{-2} near the region of maximum fluxes the percentage of heat loss is approximately 17% via air–sea fluxes. In experiment C2 without the WCR, the maximum flux remains just over 1500 W m^{-2} without the contribution from the WCR as a reservoir of heat (Fig. 15).

The air–sea interactions between Opal and the WCR can be further examined by using temporal variations of several key parameters in the interaction of Opal and the WCR. These parameters—depth of 26°C isotherm, ocean heat content, surface heat fluxes, and the surface wind stress—are normalized [$x_1(t)$] by their maximum and minimum values,

$$x_1(t) = \frac{x(t) - x_{\min}}{x_{\max} - x_{\min}}, \tag{7}$$

due to their large difference in magnitude. In the above expression, $x(t)$ is the value of the selected variable, and $x_{\min}$ and $x_{\max}$ are the minimum and maximum values of $x(t)$, respectively. The maximum and minimum values sampled at (25°N, 89°W) are listed in Table 2. As shown in Fig. 16, the four parameters stay relatively unchanged to 1800 UTC 3 October before Opal encounters the WCR. Then both the total heat flux and wind stress increase suddenly to 60%–70% of their respective maximum values at 0600 UTC 4 October as the northern

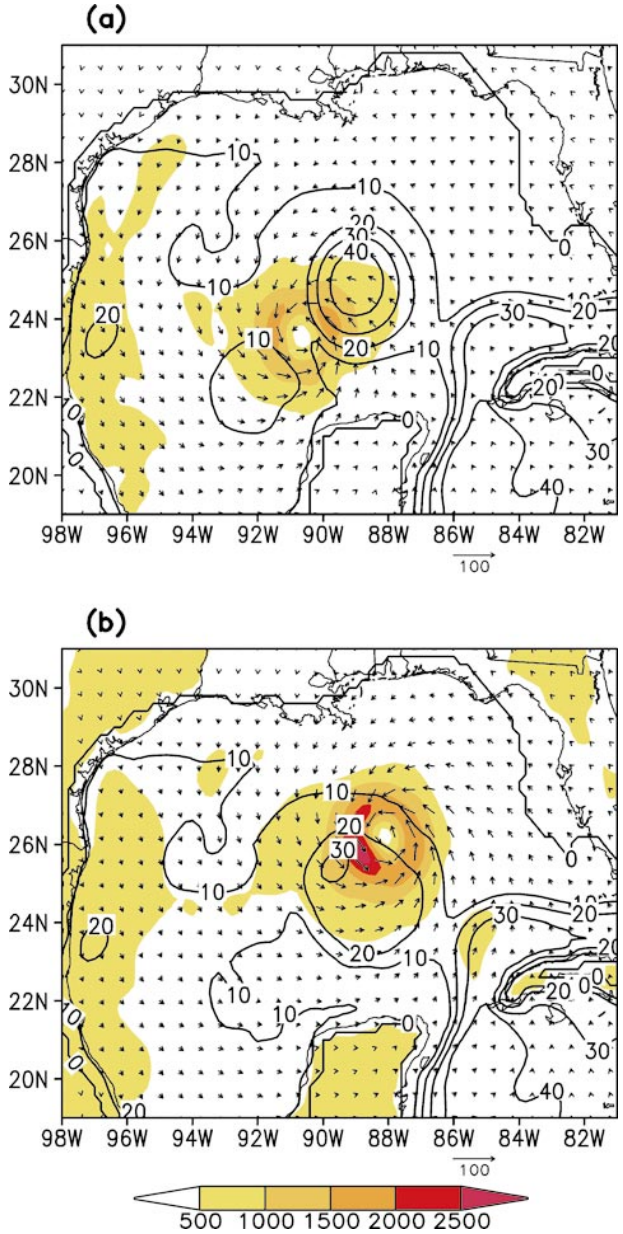

FIG. 14. Surface wind vectors (m s^{-1}), sensible and latent heat fluxes (shaded) in W cm^{-2}, and the upper ocean heat content (contour) in kcal cm^{-2} at (a) 0000 UTC 4 Oct and (b) 1800 UTC 4 Oct for heat fluxes and 0000 UTC 5 Oct for heat content for expt C1. The contour interval is 10 kcal cm^{-2}.

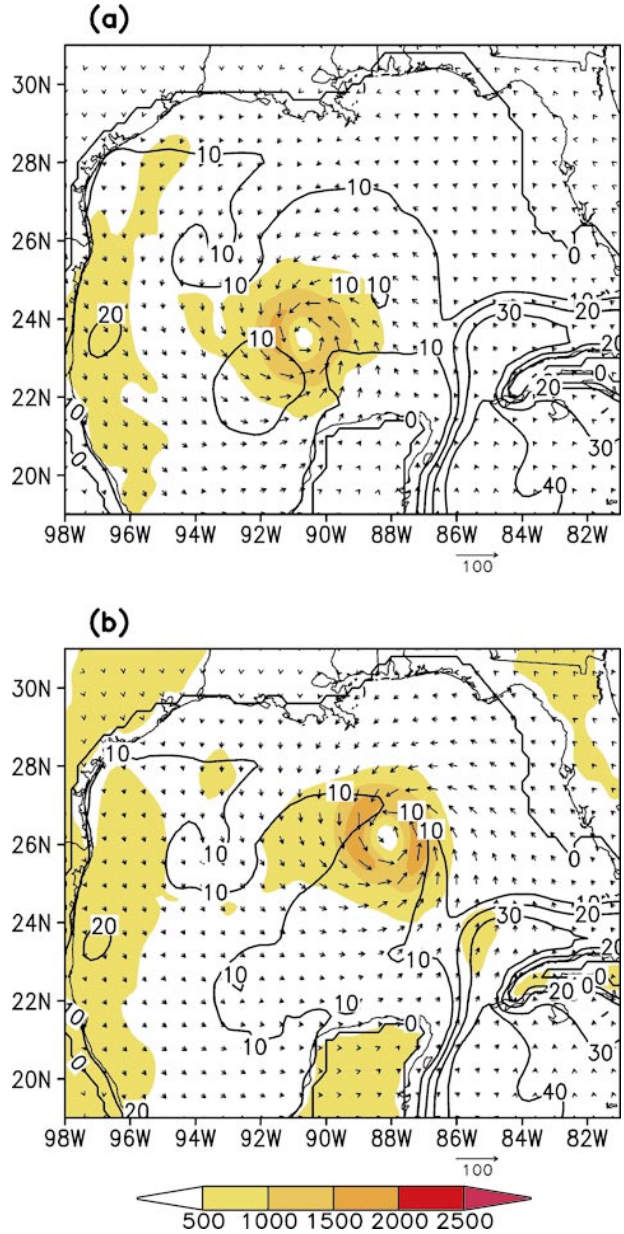

FIG. 15. Same as Fig. 14 except for expt C2.

eyewall moves over the sampling point at 25°N, 89°W. Prior to this time, the loss of the total heat content is only 15% of the total loss. This very large decrease and increase signifies the passing of the eye and the southern section of the eyewall of Opal. During this rapid change, the heat flux and wind stress increase by 1313 W m^{-2} and 10 dyn cm^{-2} from the prestorm levels and attain their maximum values of 2597 W m^{-2} and approximately 82 dyn cm^{-2} at approximately 1500 UTC 4 October. The difference in the heat content over a 15-h period is about 20 units or approximately 15.5 kW m^{-2}. Given the surface heat flux of 2597 W m^{-2}, the loss of heat to the atmosphere is 16%–17%. Shay et al. (2000) differenced pre- and post-Opal TOPEX images and found the heat content change based upon a gradient method was approximately 24 units. Given the range of heat losses to the atmosphere by Black (1983) of 10%–15%, the inferred surface heat flux ranged between 2000 and 3000 W m^{-2} assuming that the large heat content loss occurred over a 14-h period. This inferred surface heat flux is in agreement with the maximum found in the simulations. The total heat content and the mixed layer depth both have small increases between 0000 and

TABLE 2. The maximum and minimum values of $x(t)$ at (25°N, 89°W).

	Depth of 20°C isotherm (m)	Heat content (kcal cm^{-2})	Heat fluxes (W m^{-2})	Wind stress (dyn cm^{-2})
Max (expt C1)	200	46	2597	82
Max (expt C2)	71	8	1711	7
Min (expt C1)	129	27	0	0
Min (expt C2)	0	0	0	0

1200 UTC 4 October due to the prestorm downwelling of the mixed layer. Rapid decreases of the mixed layer depth and total heat content coincide with the eye's arrival due to Ekman-induced upwelling of cooler thermocline water. At this time the ocean is spun up and the strong stress field is most efficient in inducing vertical mixing at $2R_{max}$ and upwelling along the track. Notice that the difference between pre- and poststorm isotherm depth is about 70 m. The differences between the pre- and post-Opal TOPEX imagery was about 50 m, which was based on a simple two-layer model approach compared to the high-resolution vertical structure in this model. After the passing of Opal at the sampling point, starting from 0000 UTC 5 October, the recovery of the WCR begins.

Without the WCR, the temporal variations of the heat content in experiment C2 (Fig. 17) is not as dramatic as compared to that in C1 shown in Fig. 16. The available heat content defined in (6) is only approximately 10 kcal cm^{-2} at the same sampling point at 25°N, 89°W. The maximum heat flux in C2 is 1711 W m^{-2}, 30% less than that in experiment C1.

The net ocean response in the Gulf of Mexico with the absence of the WCR in experiment C2 differs from experiment C1 as anticipated. Without the anticyclonic circulation associated with WCR, there exists only very weak, less organized current in the prestorm Gulf. The induced surface current field in C2 is very similar to results of earlier idealized simulations (e.g., Chang and Anthes 1978; Price 1981; Shay et al. 1990). The poststorm SST (Fig. 18) features a more continuous cold pool to the right of the track, extended over the location of the WCR in experiment C1 (Fig. 10). The wind-induced cooling in C2 is up to 0.5°C stronger over and to the north of the WCR location.

e. Feedback effects

We have discussed the interactions between Hurricane Opal and the Gulf of Mexico in the presence of a WCR. The behavior of Hurricane Opal is undoubtedly coupled to the underlying SST. The effect of the *feedback* of the induced ocean response is examined, mainly, the SST cooling, to an overlying tropical cyclone. (This is not to be confused with the response of tropical cyclone to varying SST field.) Conversely, we can also examine the effect of the tropical cyclone weakening, due to the ocean response, on the ocean. However, the feedback to ocean is more obvious and its magnitude has less societal impact and, therefore, is precluded from the scope of this paper. As discussed above, there have been several idealized studies on this issue. In general, the feedback is found to be negative, but the tropical cy-

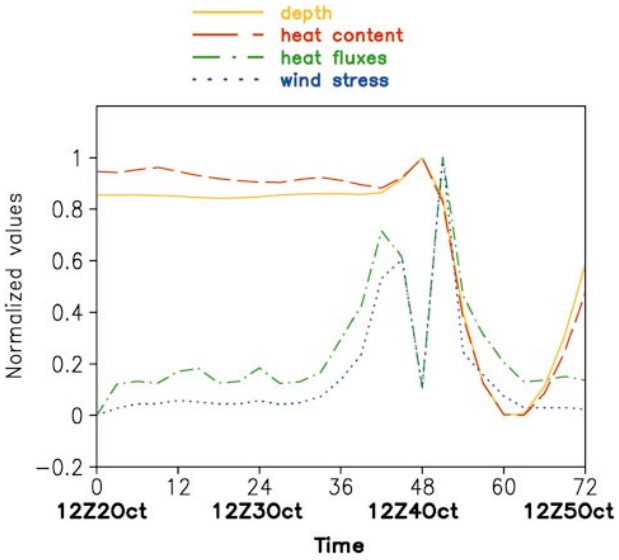

FIG. 16. Normalized variables including the depth of the 26°C isotherm, ocean heat content, surface heat fluxes, and the surface wind stress for expt C1. The maximum and minimum values for normalization are listed in Table 2.

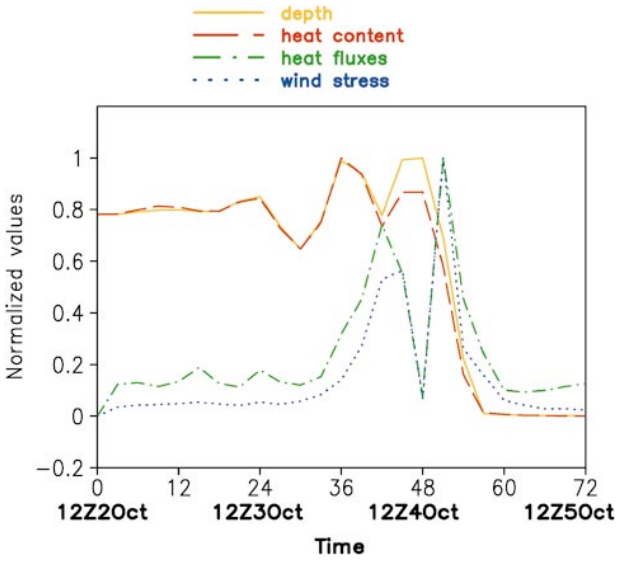

FIG. 17. Same as Fig. 16 except for expt C2.

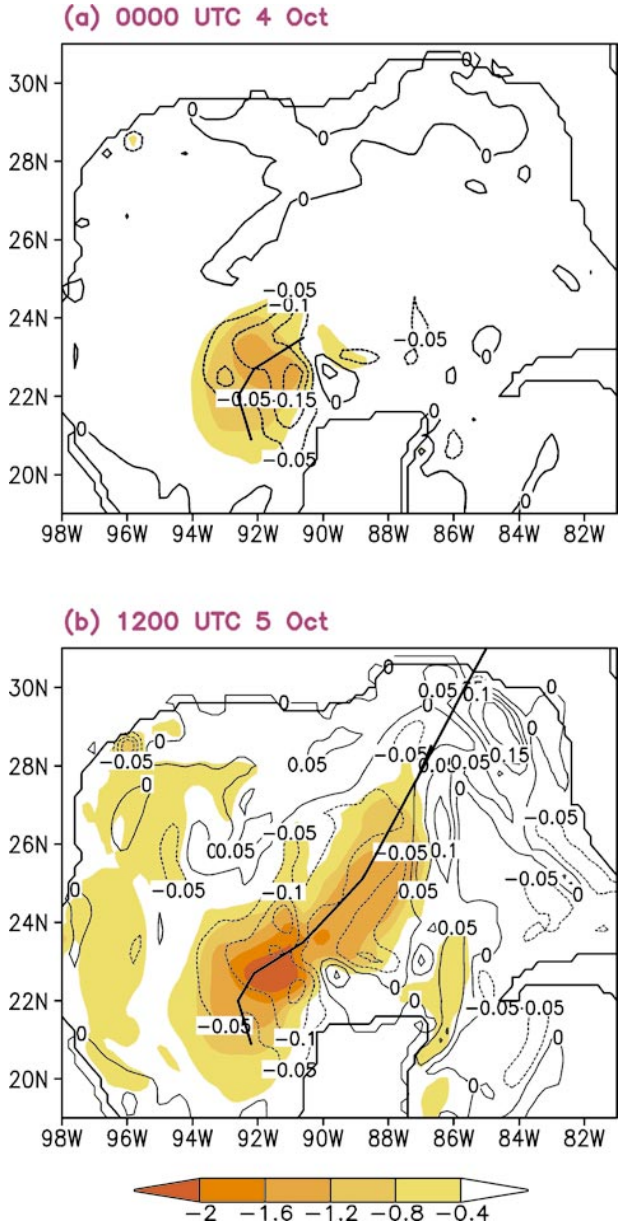

FIG. 18. Changes of the sea surface temperature (shaded) and the sea surface salinity (contours) at (a) 0000 UTC 4 Oct and (b) 1200 UTC 5 Oct for expt C2.

clone response particularly under quiescent ocean conditions varies due to differing sensitivities to SST in tropical cyclone models.

Two numerical integrations of the atmospheric component from the coupled model are conducted to elucidate the effect of the feedback between Opal and the Gulf of Mexico. Experiment U1 is run in which the initial SST with the WCR (Fig. 5) is held constant throughout the integration, whereas experiment U2 is run with the initial SST without the WCR. The minimum SLPs of the simulated Opal are plotted in Fig. 12.

Comparing C1 and U1, the effect of coupling to the ocean on Opal is small, albeit noticeable, after the first 24 h of integration. At the maximum intensity at around 1800 UTC 4 October for both experiments, the difference is 5 hPa (Table 3). *This is not to be interpreted that Hurricane Opal is insensitive to the SST, it is merely that the effect of the feedback from the cooled ocean makes Opal 5 hPa weaker.* That is, less heat is available for Opal because of storm-induced mixing and active entrainment across the mixed layer base, which in turn lowers the heat fluxes. Examining the induced SST changes in Fig. 11, the average cooling within 200 km of the track is on the order of 1°C as anticipated for a fast-moving storm (i.e., time available for vertical mixing is short). In Emanuel (1988), the sensitivity of the intensity of a steady-state tropical cyclone to prescribed SST field in an uncoupled model is -6 hPa K^{-1}. The 5-hPa difference in experiments C1 and U1 agrees well with this theoretical result.

TABLE 3. The differences of the lowest minimum sea level pressure (hPa) between the experiments.

Expts	C1–U1	C2–U2	C1–C2	U1–U2	U1–U3	U2–U3
HPa	5	7	−10	−8	−1	7

The feedback effect without the presence of WCR can be examined by comparing experiments C2 and U2. As shown in Fig. 12, the maximum intensity is 8 hPa at 0000 UTC 5 October. *The negative feedback effect is stronger without the presence of the WCR.* The average induced SST cooling near the track is closer to 1.5°C in experiment C2 (Fig. 18). It is evident that the warm, deeper isothermal layers in a WCR do not significantly decrease the ocean thermal response, which reduces the negative feedback effect to the tropical cyclone. The magnitude of feedback is again consistent with Emanuel's theory and with numerical experiments with the WCR.

6. Summary and discussion

A coupled atmosphere and ocean model, the atmospheric component of COAMPS and MOM2, has been used to investigate the interaction between Hurricane Opal (1995) and the Gulf of Mexico in early October of 1995 as described by Marks et al. (1998). Hurricane Opal moved directly over a WCR shed from the Loop Current during a favorable upper-atmospheric trough interaction (Bosart et al. 2000). The sea surface temperature signature of the WCR was in general masked by insolation, but the deep warm water mass of the WCR acts as a large heat reservoir for tropical cyclones and a source of enhanced latent and sensible heat release.

A control numerical experiment was first conducted in which the atmosphere was allowed to interact with the ocean. The simulated Opal moved slower and took a path slightly to the east of the observed storm track, placing itself directly over the WCR. The central pres-

sure decreased from the initial 985 hPa to a minimum of 917 hPa in 54 h as the storm center exited the northern edge of the WCR. Due to the slower-than-observed movement of the simulated storm, the maximum intensity was reached 6 h later than the observed maximum. The weakening also occurred later than observed. The maximum SLP tendencies during the deepening and weakening period were similar to the observed SLP, but the evolution of the minimum SLP of the simulated storm was less dramatic (Fig. 8). The thermal and dynamic response of the Gulf of Mexico was similar to earlier idealized simulations, except over the WCR where the maximum SST decrease was about 0.5°C as compared to the 2°C cooling elsewhere. Shay et al. (2000) reported on buoy measurements in the WCR during Opal's passage where SSTs changed by only 0.5°C. The induced surface current field in the wake was altered by the anticyclonic circulation around the WCR, which was temporarily turned into cyclonic rotation in the front half of Hurricane Opal as it passed over the feature. Shay et al. (1998) showed that the circulation associated with the WCR had to be removed from current profiles to resolve the near-inertial wave response to Gilbert.

Further analyses and additional numerical experiments indicated that approximately 40% of the available heat content of the WCR was extracted by Opal via enhanced air–sea fluxes. The heat transfer was converted into an increase of grid-scale precipitation (hence higher equivalent potential temperatures) and into an intensification of Opal. The WCR is responsible for 60% of the intensification of 17 hPa when Opal interacted with the WCR. A series of uncoupled numerical experiments were also conducted. As expected, the uncoupled experiments resulted in stronger intensity of Opal and stronger ocean response. Uncoupled experiments suggested that the negative feedback of the induced ocean response to Opal was on the order of 5–8 hPa. Considering the average induced SST cooling, the feedback agreed with the linear theory. It is worth noting that *the hurricane–ocean coupling is stronger (i.e., stronger interfacial fluxes) but the negative feedback is weaker in the case with the WCR* due to its deeper and warmer isothermal layers.

The results presented consist of a simple coupling between Opal and the Gulf of Mexico during the time window of our simulation from 2 October 1995; namely, no looping occurred nor did a second hurricane move into the Gulf. In more complicated cases, the feedback from the ocean can be considerably more significant. In this study, only the importance of the large upper ocean heat content from the WCR in the Gulf of Mexico on intensifying hurricane Opal has been studied. The complete mechanisms responsible for Opal's track, speed, and rapid intensification still remain to be investigated. What are the relative roles played by the storm's inner core dynamics, upper-level trough, and upper-ocean heat content from the WCR on the significant intensity change? The relative importance of the upper-tropospheric dynamics on the rapid intensification of Opal still remains an interesting scientific question to be explained.

Initial conditions must be carefully set up in conducting coupled numerical experiments. In our case, the initial condition for the atmosphere model was derived from the archived NOGAPS operational global analysis field, which was enhanced with observations within the model domain by a multivariate optimum interpolation data assimilation scheme. The inner structure of Opal was not well resolved, resulting in a difference of 10 hPa in the initial MSLP. This may have contributed to the slower speed. The effort to obtain the initial condition for the ocean model was, however, much more difficult due to the lack of any ocean ''analysis'' for October 1995. Initial conditions for the regional ocean model had to be generated by a 2-yr MOM2 simulation with climatological forcing with a fixed mass inflow at the lateral boundaries derived from a 2-yr global MOM2 simulation. The initial oceanic state in the Gulf of Mexico, even though consisting of quite realistic features of the Loop Current and the WCR, was not analyzed using any observations. Given that, the agreement with the observed ocean response derived from remotely sensed fields and buoy measurements (Shay et al. 2000) was fortunate. It would be impossible to conduct coupled numerical or forecast experiments of many historical cases in different basins without corroborating profiles or buoy measurements in both geophysical fluids. It is hoped that advancement in remote sensing and in situ observational technologies (Marks et al. 1998) and data assimilation technique will help to gain more insight of the initial states of the atmosphere and the ocean.

In addition to the difficulties in obtaining the initial conditions discussed above, numerical models used in this study, both atmosphere and ocean, can be improved, especially in spatial resolutions and boundary layer parameterizations and the condensation process. Fortunately, the atmospheric component of the coupled system used in this study, COAMPS, is used operationally at the Fleet Numerical Meteorology and Oceanography Center and other navy regional centers; therefore, it will be further improved and validated. Similar scrutiny should also be applied to the ocean component, or any other ocean model. This study represents only an initial attempt toward a realistic simulation of the interaction between tropical cyclones with underlying mesoscale ocean features. It is necessary that continuous effort be undertaken to observe, model, and analyze this complex phenomenon.

The importance of coupled model in the hurricane forecast is obvious, especially when there are large spatial variations of surface and subsurface ocean thermal content. These variations can modulate tropical cyclone intensity as shown by this study, which hopefully will provide an impetus for improved parameterizations for interfacial transfers, especially for high wind conditions.

It is clear from our study that accurate and frequent analyses of sea surface and subsurface structure, and an adequate description of their temporal changes are indispensable components for accurate numerical tropical cyclone intensity forecasting.

Acknowledgments. The authors thank many people at NRL Monterey for their contributions to this work: Dr. Tianming Li provided an early version of GFDL MOM2. Mrs. Sue Chen Schmidt helped to implement the GFDL MOM2 into the COAMPS software library; the NOGAPS global atmospheric datasets were kindly prepared by Dr. Timothy Hogan, Dr. Teddy Holt, and Mr. Robert Godfrey; Dr. Jim Cummings supplied the objectively analyzed AVHRR SST. The first authors had many helpful discussions with Drs. Liang Xu, James Doyle, Ed Barker, and Jerome Schmidt on various aspects of the work. Mr. Pedro Tsai and Mr. Gary Love helped on using GrADS. Finally, we thank Dr. Gustavo Goni (NOAA/AOML/PhOD) for the TOPEX imagery. This research was supported by NRL Basic Research Program PE601153N and the ONR 6.2 program PE602435N. The computations were performed at the Naval Oceanographic Office (NAVOCEANO) of the Department of Defense Major Shared Resource Center. LKS was supported by ONR Grant N00014-93-1-0417 and NSF/NOAA Grant ATM-97-14885.

REFERENCES

Anthes, R. A., and S. W. Chang, 1978: Response of the hurricane boundary layer to changes of sea surface temperature in a numerical model. *J. Atmos. Sci.,* **35,** 1240–1255.

Bender, M. A., I. Ginis, and Y. Kurihara, 1993: Numerical simulations of tropical cyclone–ocean interaction with a high resolution coupled model. *J. Geophys. Res.*, **98,** 23 245–23 263.

Black, P. G., 1983: Ocean temperature changes induced by tropical cyclones. Ph.D. dissertation, The Pennsylvania State University, 278 pp. [Available from Department of Meteorology, Pennsylvania State University, University Park, PA 16802.]

Bosart, L., C. S. Velden, W. E. Bracken, J. Molinari, and P. G. Black, 2000: Environmental influences on the rapid intensification of Hurricane Opal (1995) over the Gulf of Mexico. *Mon. Wea. Rev.*, **128,** 322–352.

Brand, S., 1971: The effects on tropical cyclones of cooler surface waters due to upwelling and mixing produced by a prior tropical cyclone. *J. Appl. Meteor.,* **10,** 865–874.

Brooks, D., 1983: The wake of Hurricane Allen in the western Gulf of Mexico. *J. Phys. Oceanogr.,* **13,** 117–129.

Bryan, K., 1969: A numerical method for the study of the circulation of the World Ocean. *J. Comput. Phys.,* **4,** 347–376

Chang, S. W., and R. A. Anthes, 1978: Numerical simulations of the ocean's nonlinear, baroclinic response to translating hurricanes. *J. Phys. Oceanogr.,* **8,** 468–480.

——, and ——, 1979: The mutual response of the tropical cyclone and the ocean. *J. Phys. Oceanogr.,* **9,** 128–135.

Cox, M. D., 1984: A primitive equation, 3-dimensional model of the ocean. GFDL Ocean Group Tech. Rep. 1, 75 pp. [Available from NOAA/Geophysical Fluid Dynamics Laboratory, Princeton University, Princeton, NJ 08542.]

Davies, H. C., 1976: A lateral boundary formulation for multi-level prediction models. *Quart. J. Roy. Meteor. Soc.,* **102,** 405–418.

——, 1983: Limitations of some common lateral boundary schemes used in regional NWP models. *Mon. Wea. Rev.,* **111,** 1002–1012.

Deardorff, J. W., 1980: Stratocumulus-capped mixed layers derived from a three-dimensional model. *Bound.-Layer Meteor.,* **18,** 495–527.

DeMaria, M., and J. Kaplan, 1994: Sea surface temperature and the maximum intensity of Atlantic tropical cyclones. *J. Climate,* **7,** 1324–1334.

Emanuel, K. A., 1986: An air–sea interaction theory for tropical cyclones. Part I: Steady-state maintenance. *J. Atmos. Sci.,* **43,** 585–604.

——, 1988: The maximum intensity of hurricanes. *J. Atmos. Sci.,* **45,** 1143–1155.

Esbensen, S. K., and Y. Kushnir, 1981: The heat budget of the global ocean: An atlas based on estimates from surface marine observations. Climatic Research Institute and Department of Atmospheric Sciences Rep. 29, Oregon State University, Corvallis, OR, 27 pp. [Available from Climate Research Institute and Department of Atmospheric Sciences, Oregon State University, Corvallis, OR 97331.]

Fisher, E. L., 1958: Hurricane and the sea surface temperature field. *J. Meteor.,* **15,** 328–333.

Ginis, I., and G. Sutyrin, 1995: Hurricane-generated depth-averaged currents and sea-surface elevation. *J. Phys. Oceanogr.,* **25,** 1218–1242.

Goerss, J. S., and R. A. Jeffries, 1994: Assimilation of synthetic tropical cyclone observations into the Navy Operational Global Atmospheric Prediction System. *Wea. Forecasting,* **9,** 557–576.

——, C. S. Velden, and J. D. Hawkins, 1998: The impact of multispectral *GOES-8* wind information on Atlantic tropical cyclone track forecasts in 1995. Part II: NOGAPS forecasts. *Mon. Wea. Rev.,* **126,** 1219–1227.

Harshvardhan, R. Davies, D. Randall, and T. Corsetti, 1987: A fast radiation parameterization for atmospheric circulation models. *J. Geophys. Res.,* **92,** 1009–1015.

Hodur, R. M., 1997: The Naval Research Laboratory's Coupled Ocean/Atmosphere Mesoscale Prediction System (COAMPS). *Mon. Wea. Rev.,* **125,** 1414–1430.

Jacob, S. D., L. K. Shay, A. J. Mariano, and P. G. Black, 2000: The 3D oceanic mixed layer response to Hurricane Gilbert. *J. Phys. Oceanogr.,* in press.

Kain, J. S., 1990: A one-dimensional entraining–detraining plume model and its application in convective parameterization. *J. Atmos. Sci.,* **47,** 2784–2802.

——, and J. M. Fritsch, 1993: Convective parameterization for mesoscale models: The Kain–Fritsch scheme. *The Representation of Cumulus Convection in Numerical Models, Meteor. Monogr.,* No. 46, Amer. Meteor. Soc., 165–170.

Klemp, J., and R. Wilhelmson, 1978: The simulation of three-dimensional convective storm dynamics. *J. Atmos. Sci.,* **35,** 1070–1096.

Lai, D. Y., and T. B. Sanford, 1986: Observations of hurricane generated slope modes. *J. Phys. Oceanogr.,* **16,** 657–666.

Leipper, D., 1967: Observed ocean conditions and hurricane Hilda, 1964. *J. Atmos. Sci.,* **24,** 182–196.

Levitus, S., 1982: *Climatological Atlas of the World Ocean.* NOAA Prof. Paper 13, U.S. Government Printing Office, Washington, DC, 173 pp.

Lorenc, A. C., 1986: Analysis methods for numerical weather prediction. *Quart. J. Roy. Meteor. Soc.,* **112,** 1177–1194.

Louis, J. F., M. Tiedtke, and J. F. Geleyn, 1982: A short history of the operational PBL-parameterization at ECMWF. Preprints, *Workshop on Planetary Boundary Parameterization,* Reading, United Kingdom, ECMWF, 59–79.

Marks, F., L. K. Shay, and PDT-5, 1998: Landfalling tropical cyclones: Forecast problems and associated research opportunities. *Bull. Meteor. Soc.,* **79,** 305–323.

Martinsen, E. A., and H. Engedahl, 1987: Implementation and testing of a lateral boundary scheme as an open boundary condition in a barotropic ocean model. *Coastal Eng.,* **11,** 603–627.

Miller, B. I., 1958: On the maximum intensity of hurricanes. *J. Meteor.,* **15,** 184–195.

Namias, J., 1976: Negative ocean-air feedback systems over the North Pacific in the transition from warm to cold seasons. *Mon. Wea. Rev.,* **104,** 1107–1121.

Pacanowski, R. C., 1996: MOM 2 (version 2.0) documentation user's guide and reference manual. GFDL Ocean Tech. Rep. 3.2, 329 pp. [Available from NOAA/Geophysical Fluid Dynamics Laboratory, Princeton University, Princeton, NJ 08542.]

——, and G. Philander, 1981: Parameterization of vertical mixing in numerical models of the tropical ocean. *J. Phys. Oceanogr.,* **11,** 1442–1451.

Perlroth, I., 1967: Hurricane behavior as related to oceanographic environmental conditions. *Tellus,* **19,** 258–267.

——, 1969: Effects of oceanographic media on equatorial Atlantic hurricanes. *Tellus,* **21,** 230–244.

Price, J. F., 1981: Upper ocean response to a hurricane. *J. Phys. Oceanogr.,* **11,** 153–175.

Rutledge, S. A., and P. V. Hobbs, 1983: The mesoscale and microscale structure of organization of clouds and precipitation in midlatitude cyclones. VIII: A model for the ''seeder-feeder'' process in warm-frontal rainbands. *J. Atmos. Sci.,* **40,** 1185–1206.

Semtner, A. J., 1974: A general circulation model for the World Ocean. UCLA Dept. of Meteorology Tech. Rep. 8, 99 pp. [Available from Department of Marine, Earth and Atmospheric Sciences, Box 8208, North Carolina State University, Raleigh, NC 27695.]

Shay, L. K, S. W. Chang, and R. L. Elsberry, 1990: Free surface effects on the near-inertial current response to a hurricane. *J. Phys. Oceanogr.,* **20,** 1405–1424.

——, P. G. Black, A. J. Mariano, J. D. Hawkins, and R. L. Elsberry, 1992: Upper ocean response to Hurricane Gilbert. *J. Geophys. Res.,* **97,** 20 227–20 248.

——, A. J. Mariano, S. D. Jacob, and E. H. Ryan, 1998: Mean and near-inertial ocean current response to Hurricane Gilbert. *J. Phys. Oceanogr.,* **28,** 858–889.

——, G. J. Goni, and P. G. Black, 2000: Effects of a warm oceanic feature on Hurricane Opal. *Mon. Wea. Rev.,* **128,** 1366–1383.

Sturges, W., J. C. Evans, S. Welsh, and W. Holland, 1993: Separation of warm-core rings in the Gulf of Mexico. *J. Phys. Oceanogr.,* **23,** 250–268.

Sutyrin, G. G., and A. P. Khain, 1984: Effect of the ocean–atmosphere interaction on the intensity of a moving tropical cyclone. *Atmos. Oceanic Phys.,* **20,** 697–703.

Tisdale, C. F., and P. F. Clapp, 1963: Origin and paths of hurricanes and tropical storms related to certain physical parameters at the air–sea interface. *J. Appl. Meteor.,* **2,** 358–367.

Vukovich, F. M., and G. A. Maul, 1985: Cyclonic eddies in the eastern Gulf of Mexico. *J. Phys. Oceanogr.,* **15,** 105–117.

——, M. Bushnell, and W. J. King, 1979: Some aspects of the oceanography of the Gulf of Mexico using satellite and in situ data. *J. Geophys. Res.,* **84,** 7749–7768.

Xu, L., 1995: The study of mesoscale land–air–sea interaction processes using a nonhydrostatic model. Ph.D. dissertation, North Carolina State University, Raleigh, 336 pp. [Available from Department of Meteorology, University of California, Los Angeles, CA 90095.]